 doi:10.20944/preprints202209.0342.v1

Article

A Novel Anoikis-Related Gene Signature Predicts Prognosis in Patients with Low-Grade Glioma and Reveals Immune Infiltration

Songyun Zhao [1,†], Hao Chi [2,†], Wei Ji [1,†], Qisheng He [1], Guichuan Lai [3], Gaoge Peng [2], Xiaoyu Zhao[4], Chao Cheng [1,*], Weiyi Huang [1,*]

[1] Department of Neurosurgery, Wuxi People's Hospital Affiliated to Nanjing Medical University, Wuxi 214000, China; 2021122190@stu.njmu.edu.cn(S.Z), wxrmyyjw@163.com(W.J.), 18021640216@163.com(Q.H.), Mr_chengchao@126.com(C.C.), weiy_huang@126.com (W.H.)

[2] Clinical Medicine college, Southwest Medical University, Luzhou,646000, China; Chihao7511@163.com (H.C.), penggaoge@yeah.net (G.P.)

[3] Department of Epidemiology and Health Statistics, School of Public Health, Chongqing Medical University, Yixue Road, Chongqing 400016, China;2020111425@stu.cqmu.edu.cn(G.L.)

[4] Department of Neurosurgery, The First Affiliated Hospital of Xinjiang Medical University, Urumqi 830054, China; z1482582421@163.com(X.Z.)

†These authors have contributed equally to this work.

* Correspondence: Mr_chengchao@126.com(C.C.); Tel: +86 13812056275; weiy_huang@126.com (W.H.); Tel: +86 13806184166

Abstract: Low-grade glioma (LGG) is a highly aggressive disease in the skull. On the other hand, anoikis, a specific form of cell death induced by the loss of cell contact with the extracellular matrix, plays a key role in cancer metastasis. In this study， anoikis-related genes (ANRGs) were used to identify LGG subtypes and to construct a prognostic model for LGG patients. In addition, we explored the immune microenvironment and enrichment pathways between different subtypes. We constructed an anoikis-related gene signature using the TCGA cohort and investigated the differences in clinical features, mutational landscape, immune cell infiltration, etc. between different risk groups. Kaplan-Meier analysis showed that the characteristics of ANRGs in the high-risk group were associated with poor prognosis in LGG patients. The risk score was identified as an independent prognostic factor. The high-risk group had higher immune cell infiltration, tumor mutation load, immune checkpoint gene expression, and ICB treatment response. Functional analysis showed that these high- and low-risk groups had different immune statuses and drug sensitivity. Risk scores were used together with LGG clinicopathological features to construct a nomogram, and DCA analysis showed that the model could enable patients to benefit from clinical treatment strategies.

Keywords: anoikis; Low-grade glioma; signature; prognosis; immune microenvironment

1. Introduction

Glioma is a relatively common primary tumor in the brain that originates mainly from glial cells in the brain tissue, and low-grade gliomas (LGG) account for about one-third of all gliomas[1]. Low-grade glioma (LGG) is a diffusely infiltrating, slow-growing glial brain tumor that tends to have extensive genetic and transcriptional heterogeneity[2]. According to the Cancer Genome Atlas Project classification, "low-grade glioma" has taken the place of the phrase "lower grade glioma," which was formerly often used to refer to grade 2 gliomas[3]. LGG is usually considered to have a benign course, however, diffuse low-grade gliomas (LGG) naturally transform into malignant high-grade gliomas, and once recurring and progressing to high-grade gliomas, they can greatly limit patient survival[4]. The poor prognosis and mortality associated with glioma are mainly due to the highly aggressive and mobile nature of the tumor cells, which can spread and spread

 doi:10.20944/preprints202209.0342.v1

widely into the surrounding brain tissue[5]. To date, the molecular mechanisms of glioma invasion and migration are not fully understood[6]. The epithelial-mesenchymal transition (EMT) of glioma cells is a significant component contributing to the aggressiveness of high-grade gliomas. For prompt clinical interventions to halt the growth of the disease, more novel biomarkers are urgently required at an early stage to predict the prognosis of glioma patients.

In the absence of extracellular matrix (ECM) attachment or when cells adhere to inappropriate sites, cells undergo a specific type of apoptosis called anoikis[7,8]. anoikis acts as an important defense for the organism by preventing shedding cells from re-adhering to incorrect locations and preventing their growth[7,9]. anoikis is becoming a hallmark of cancer cells and contributes to the formation of metastases in distant organs[10,11]. However, few studies have focused on the relationship between the process of anoikis and distant metastasis of LGGs.

As a result, we created a prognostic scoring model based on ANRGs and concentrated on investigating the prognostic significance of anoikis-related genes (ANRGs) in LGG in this work. Further research was done on the variations in tumor microenvironment across patients with this risk score. We evaluated the prognostic and immunological properties of various risk grouping groups using the 7-ANRGs signature that was created. The mechanisms underlying anoikis in LGG, as well as possible prognostic biomarkers for developing logical therapy regimens, may be better understood as a result of our findings, we are confident.

2. Materials and Methods

2.1. Gene Expression and Clinical Data Acquisition

Gene expression profiles of TCGA-LGG were downloaded from the UCSC Xena website (https://xena.ucsc.edu/). 529 LGG tissue samples were available in the TCGA cohort. Gene expression profile data for the 443 patients with low-grade gliomas in the validation model were obtained from the China Glioma Genome Atlas (CGGA) data portal (http://www.cgga.org.cn/). In addition, normal control samples were obtained from The Genotype-Tissue Expression (GTEx) website (https://www.gtexportal.org/). FPKM data was finally transformed into transcript per million (TPM). Batch correction and integration of the two sets of gene expression data were performed with the "limma" and "sva"[12]packages. Detailed flow chart is shown in Figure 1.

2.2. Acquisition of Anoikis-related Genes

A total of 358 anoikis-related genes (ANRGs) were downloaded from the GeneCard database[13](https://www.genecards.org/) and Harmonizome portals[14]. Differential expression analysis of differentially expressed genes (DEGs) was performed for the TCGA cohort and different subgroups using the R software "limma" package with | log2FC |>1.0 and FDR<0.05 as thresholds.

2.3. Functional Enrichment Analysis

Functional enrichment analysis We downloaded “c2. cp.kegg.v7.4. symbols. gmt” from the MSigDB database to carry out GSVA analysis. The “GSVA” R package was used to perform GSVA enrichment analysis[15]. In addition to this, functional enrichment analysis was performed by the "clusterProfiler" package in the R software, including Kyoto Encyclopedia of Genes and Genomes (KEGG) and Gene Ontology (GO) analysis.

2.4. Consensus Clustering

Consensus clustering was applied to identify distinct anoikis-related patterns relating to the expression of anoikis regulators by the k-means method. Thereafter, Uniform Manifold Approximation and Projection (UMAP) was used to validate the reliability of clustering with the R package “ggplot2”.

Preprints (www.preprints.org) | NOT PEER-REVIEWED | Posted: 22 September 2022 doi:10.20944/preprints202209.0342.v1

2.5. Selection of Characteristic Genes

Two machine learning algorithms: random forest and SVM-RFE[16]were used to screen for signature genes. Recursive feature elimination (RFE) in the random forest algorithm is a supervised machine learning method for ranking genes in LGGs. Predictive performance was estimated by tenfold cross-validation and genes with relative importance > 0.25 were identified as feature genes. SVM-RFE is a small-sample learning method that essentially bypasses the traditional process of induction to deduction and enables efficient "transductive inference" from training to prediction samples, simplifying the usual classification and regression problems.

2.6. Development and Validation of Prognostic Signatures

First, accurate models were developed using the R package "sva" to eliminate batch effects between TCGA and CGGA data. Variables with p-values < 0.01 were selected for the least absolute shrinkage and selection operator (LASSO) regression analysis, and the number of genes in the final risk model was reduced by the R software package "glmnet". Finally, the genes from the LASSO regression were selected for the multivariate Cox regression analysis and thus constructed according to the following equation: risk score = Σ (ð × Exp), where ð is the corresponding regression coefficient and Exp represents the expression value of each mRNA. All patients were divided into high-risk and low-risk groups according to the median risk score. Survival curves and risk maps were generated to show the survival differences and status of each patient by the R software, "survminer" and "ggrisk" packages. In addition, the CGGA cohort was used as an independent external cohort to validate the utility of the prognostic model.

2.7. Estimation of the Tumor Immune Microenvironment of the Prognostic Signature

CIBERSORT and ssGSEA R scripts were used to quantify the relative proportion of infiltrating immune cells[17]. We used CIBERSORT to estimate the proportion of immune cell types between the low-risk and high-risk groups. The sum of all estimated immune cell type scores in each sample equals 1. Meanwhile, spearman rank correlation analysis was applied to explore relationships between risk score values and immune infiltrating cells.

2.8. Tumor immune Cycle and ICB Response

We obtained the cancer-immune cycle-related gene set[18] from the website developed by Xu et al. (http://biocc.hrbmu.edu.cn/TIP/) and a set of genes positively associated with clinical response to the anti-PD-L1 drug (atezolizumab) from Mariathasan's study features[19].

2.9. Construction and Evaluation of a Predictive Nomogram

The nomogram was created using risk ratings and clinicopathological features. For internal validation to confirm the accuracy, the calibration plot was executed. DCA, or decision curve analysis, was used to evaluate the clinical net benefit.[20]. In addition, we evaluated the accuracy of risk ratings in predicting 1-year, 3-year, and 5-year OS in LGG patients by plotting subject operating characteristic curves using the R software's "timeROC" package.

2.10. Tumor Immune Single Cell Hub Database

An extensive single-cell RNA-seq database devoted to the TME is available online under the name Tumor Immune Single-Cell Hub (TISCH; http://tisch.comp-genomics.org)[21]. Utilizing this database, comprehensive research on TME heterogeneity in diverse data sets and cell types was done.

2.11. Statistical Analysis

Preprints (www.preprints.org) | NOT PEER-REVIEWED | Posted: 22 September 2022 doi:10.20944/preprints202209.0342.v1

All analyses were performed using R version 4.1.1, 64-bit6, and its support package. To calculate prognostic values and to compare patient survival in different subgroups in each dataset, Kaplan-Meier survival analysis, and the log-rank test was used. The non-parametric Wilcoxon rank sum test was used to test the relationship between the two groups for continuous variables. Kruskal-Wallis test was used as a comparison between more than two groups. Clinical characteristics of the high and low-risk groups were screened for prognostic variables using univariate and multivariate Cox regression (R package 'survival'). Correlation coefficients were examined using spearman correlation analysis. In all statistical investigations, P<0.05 was considered statistically significant.

3. Results

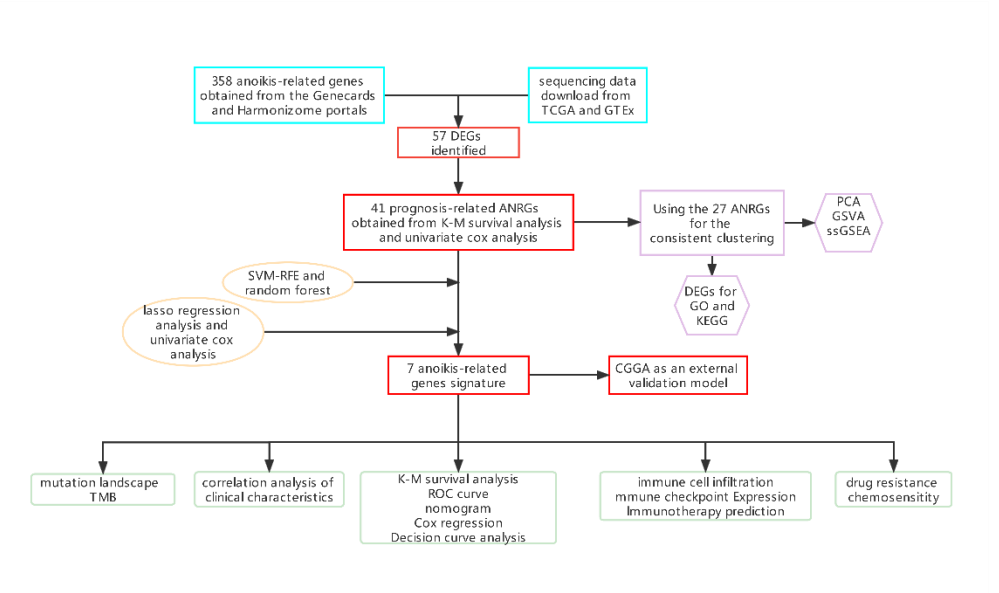

Figure 1. A detailed flow chart about the study of anoikis-related genes in LGG.

3.1. Acquisition of Anoikis-related Genes

The Genecards and Har-monizome portals yielded a total of 358 anoikis-associated genes (Supplementary Table 1), and the TCGA and CGGA cohorts included a combined total of 316 ANRGs (Figure 2A). When compared to normal adjacent tissues, we found 57 DEGs in the TCGA-LGG and GTEx cohorts, and the volcano map of these DEGs is displayed in Figure 2 B. To create the new "TCGA-CGGA" cohort, we combined the TCGA-LGG cohort with the CGGA cohort and eliminated the batch effect. 41 of 57 ANRGs were linked with survival and statistically distinct, according to univariate Cox regression analysis (p 0.05, km 0.05, Supplementary Table 2). The top 27 ANRGs most strongly correlated with prognosis in LGG patients are displayed in the forest plot (p0.001, Figure 2C) Except for ANGPTL2 and CRYAB, 25 genes were associated with poor prognosis. Meanwhile, network plots more clearly showed the relationship between the expression levels of the top 27 ranked genes (Figure 2D). Since LGG patients frequently lost or gained chromosomal regions[22], we downloaded CNV data from the TCGA database to further explore the alteration of these lost apoptosis-related genes on chromosomes and the location of each gene on chromosomes (Figure 2E, F). Figure 2F demonstrates that IFI27 was mostly displayed as a "loss" and was positioned on chromosome 14, while the most substantial changed "gain" of EGFR was located on chromosome 7.

Preprints (www.preprints.org) | NOT PEER-REVIEWED | Posted: 22 September 2022 doi:10.20944/preprints202209.0342.v1

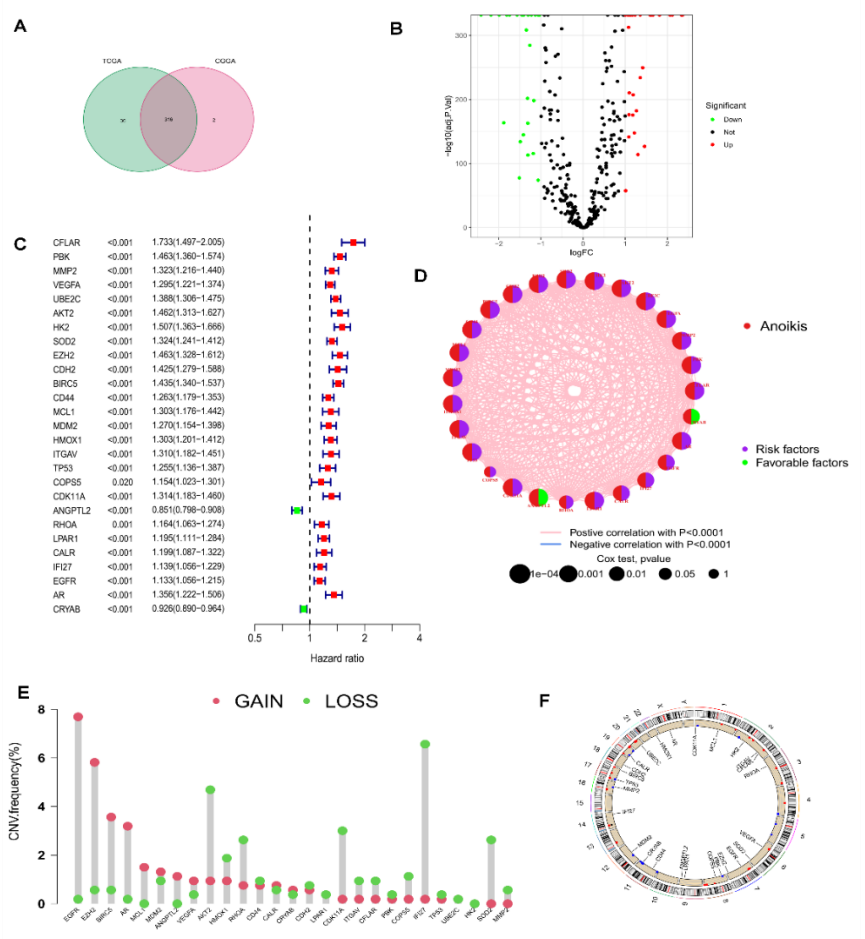

Figure 2. Characteristics of ANRGs in LGG. (A)316 anoikis-related genes identified from TCGA and CGGAcohort. (B) Volcano plot of 57 DEGs in TCGA and GTEx cohort. (C) The forest plot shows the Aanoikis-related ($p < 0.001$) via the univariate Cox regression analysis. (D) The network diagram showed the correlations between the top 27ANRGs. (E) Copy number variations (CNVs) and 27 ANRGs in TCGA-LGG. (F) Chromosome region and alteration of ANRGs.

3.2. Consistent Clustering of 27 Anoikis-related Genes in LGG

to comprehend the function of anoikis-related genes in LGG better. We used the 'Consensus Cluster Plus' R program to perform consensus clustering based on 27 prognosis-related ANRGs (P0.001) and the findings of the univariate cox analysis. When k=3, as in Figure 3A, the cohort could be effectively divided into three subtypes. A substantial difference in prognosis between the three subtypes was revealed by the overall survival analysis (P 0.001, Figure 3B). Its accuracy was examined using principal component analysis (PCA), which was used to classify the data. The findings demonstrated that, at k=3, the three clusters' subtypes could be precisely defined (Figure 3C). heat maps of ANGs expression and corresponding clinicopathological features of the 3 subtypes indicated that higher expression of ANGRs in cluster A might be associated with a worse prognosis in LGG patients, and interestingly try that very low expression of ANGs in cluster C was not associated with a better prognosis (Figure 3D), so that anoikis-related genes may regulate LGG progression through more complex pathways. We used the GSVA software to concentrate on the differential enrichment of the KEGG pathway between cluster A and cluster B given the obvious disparities between clusters A, B, and C in addition to examining the overall distribution of the 27 ANRGs in clusters (Figure 3E, Supplementary Figure 1). Cluster A with the poorest prognosis was mainly associated with the adhesive junction pathway and some common tumor-associated pathways. In glioma, adhesive linkage-associated proteins can bind to β-catenin (β-catenin) and regulate gene transcription, which

Preprints (www.preprints.org) | NOT PEER-REVIEWED | Posted: 22 September 2022 doi:10.20944/preprints202209.0342.v1

ultimately affects the cell cycle, apoptosis, and changes in cytoskeletal structure, affecting cell migration[23].

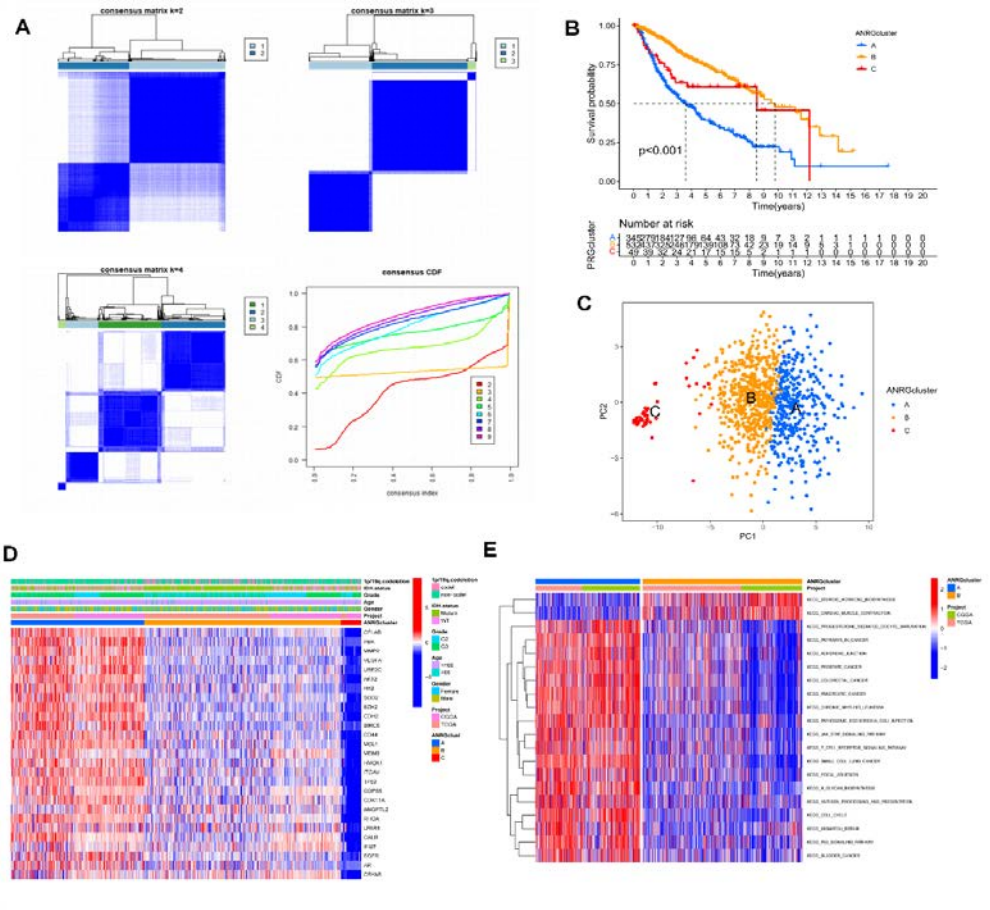

Figure 3. Subgroups of LGG related by anoikis-related genes. (A) The consensus matrix for k = 3 was obtained by applying consensus clustering. (B) Overall survival of three subtypes ($p < 0.001$). (C) PCA distinguished three subtypes based on the expression of anoikis-related genes. (D) Heat map of anoikis-related genes expression and corresponding clinicopathological features of two subtypes. (E) GSVA analysis focused on the differential enrichment of KEGG pathways between clusters A and B.

3.3. Immune infiltration and Differential Gene Expression in the Two Subtype Clusters

A boxplot was utilized to demonstrate the considerable variation in immune cell infiltration levels between the three groupings (Figure 4A). We were surprised to find that almost all percentages of immune cell infiltration were higher in group A than in groups B and C. We performed differential analysis for groups A and B, where patients had the worst survival performance, and volcano plots of the differential analysis are shown in Figure 4B. GO and KEGG enrichment analyses were performed for these differential genes, and these DEGs were associated with a variety of items, including "regulation of trans-synaptic signaling" in the biological process (BP) class, "presynapse" in the cellular component (CC) class, and molecular KEGG results showed that these genes were associated with 'proteoglycans in cancer' (Figure 4C-D), with related evidence that proteoglycans can act as co-receptors for growth factors and co-receptors for cellular matrix proteins, increasing the affinity of adhesion molecules for their specific receptors, and thus proteoglycans play an important role in the acquisition of apoptosis resistance in tumors with anoikis[24,25].

Preprints (www.preprints.org) | NOT PEER-REVIEWED | Posted: 22 September 2022 doi:10.20944/preprints202209.0342.v1

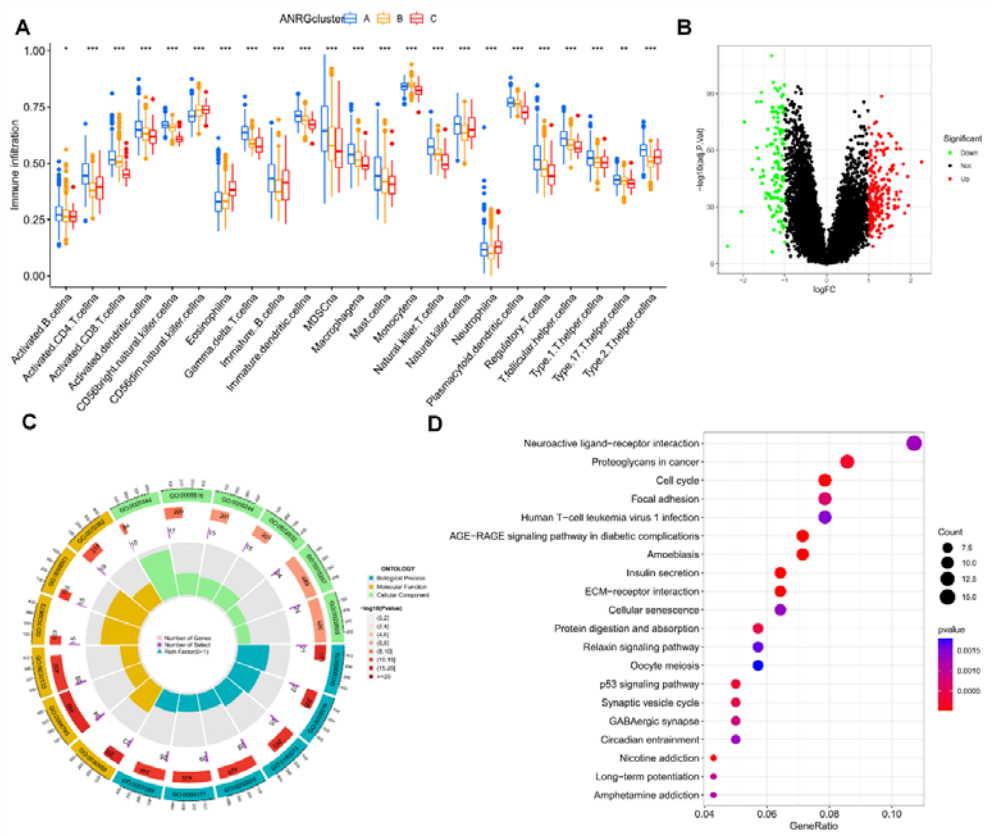

Figure 4. Differential expression of genes and immune infiltration patterns in three subtype groups. (A) Immune infiltration patterns in three subtype groups. (B) Volcano plot of up-and down-regulated DEGs in clusters A and B . (C, D) GO and KEGG enrichment analysis of DEGs.

3.4. The Development and Validationof an Anoikis-related Prognostic Signature

We used two machine learning methods to choose apoptosis-related signature genes in LGG in order to investigate the clinical utility of anoikis-related genes. For the SVM-RFE algorithm, the error was minimized when the number of features was 28 (Figure 5A). For the random forest algorithm, the 20 feature genes with the largest relative importance scores were determined (Fig. 4B, C). After taking the intersection set, 19 feature genes common to both the random forest and SVM-RFE algorithms were finally identified (Figure 5D). We then participated in a Lasso-penalized Cox analysis using these 19 ANRGs ($p<0.05$, Figure 5E, F). Finally, by multivariate Cox analysis, 7 ANRGs were identified as independent prognostic factors, including ANGPTL2, BAG1, CDH2, IFI27, PTK2B, SOD2, and UBE2C. Based on their coefficients, we calculated risk scores using the following formula.

Risk score=expression level of CDH2*0.185- expression level of ANGPTL2*0.201- expression level of the BAG1*0.167+ expression level of IFI27*0.106+ expression level of the PTK2B*0.169+ expression level of the SOD2*0.132+ expression level of UBE2C*0.308. The correlation coefficients are shown in Supplementary Table 3. Patients in the high-risk group in the TCGA-LGG cohort had a worse prognosis, according to KM curves, which was also seen in the CGGA validation cohort (Figure 5G, H). Risk plots display specific survival results for each patient in the TCGA cohort and the CGGA cohort, showing a steady rise in mortality with increasing risk scores (Fig-ure 5I, J). Risk scores were significantly different in the three previous subtypes (Figure 5K), with cluster A having a higher risk score ($P<0.01$). Alluvial plots show the association of cluster, risk, and survival status associated with ANRGs (Figure 5L).

Preprints (www.preprints.org) | NOT PEER-REVIEWED | Posted: 22 September 2022 doi:10.20944/preprints202209.0342.v1

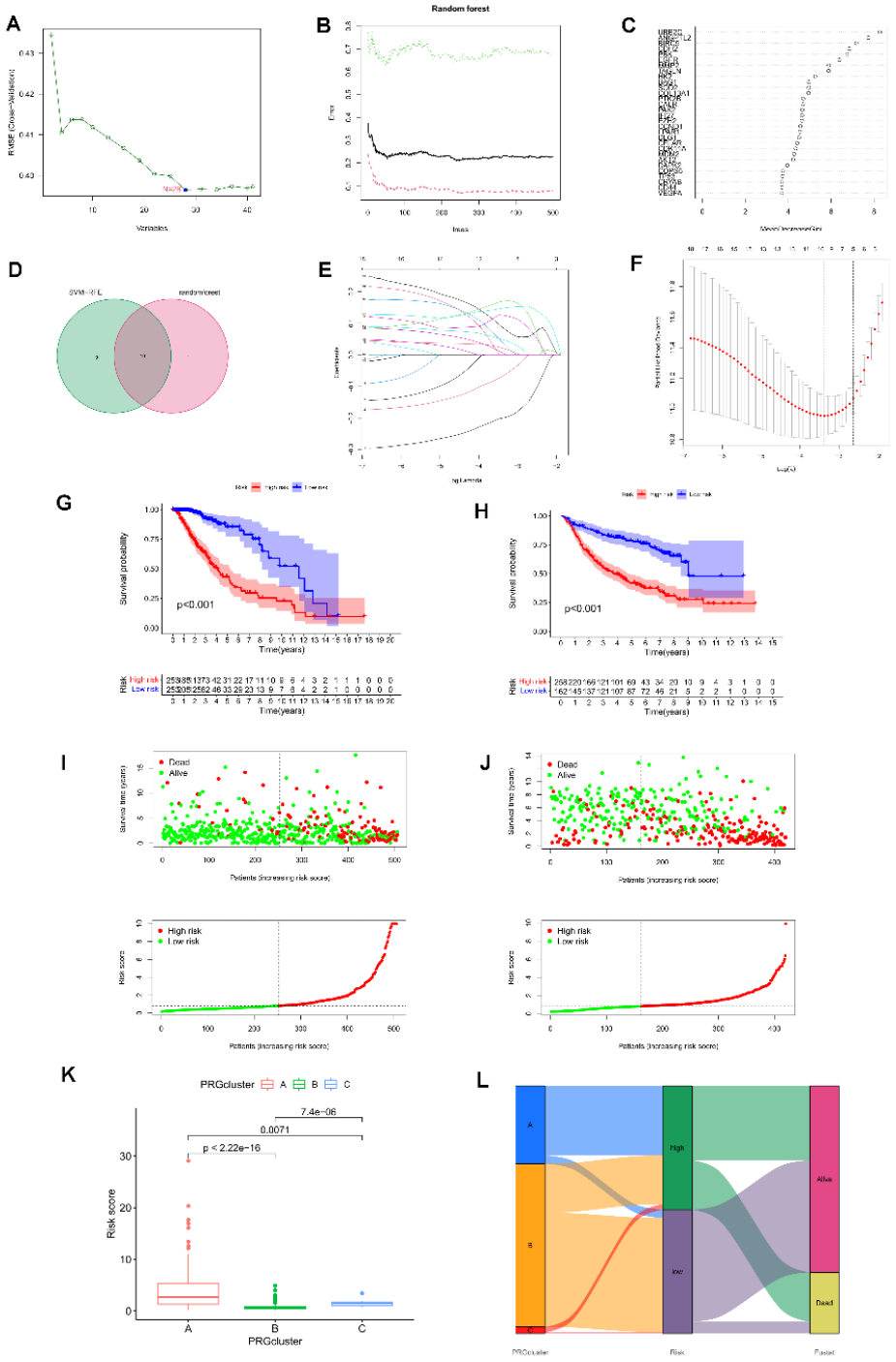

Figure 5. Identify anoikis-related prognosis signature. (A) Relationship between the number of random forest trees and error rates. (B) Ranking of the relative importance of genes. (C) SVM-RFE algorithm for feature gene selection. (D) Venn diagram showing the feature genes shared by random forest, and SVM-RFE algorithms. (E) LASSO analysis with 10-fold cross-validation identified seven prognostic genes. (F) Coefficient profile plots of seven prognostic anoikis-related genes. (G, H) The K-M curves showed a different prognosis in the subtype risk group. (I, J) Risk plots were used to illustrate the survival status of each sample in the TCGA and CGGA cohorts. (K) Risk score in 3 clusters established before. (J) Alluvial diagram of subtype and living status.

3.5. Immune Infiltration in Different Risk Groups

The development of gliomas and the effectiveness of immunotherapy are both significantly influenced by the immune microenvironment. In order to achieve this, we looked more closely at the tumor microenvironment (TME) of LGG patients. The relative

Preprints (www.preprints.org) | NOT PEER-REVIEWED | Posted: 22 September 2022 doi:10.20944/preprints202209.0342.v1

proportions of invading immune cells in the high-risk and low-risk groups were measured using the "CIBERSORT". First, the risk scores for the LGG samples were ranked from low to high to display the proportion of various immune cells (Figure 6A). With an increasing risk score, the proportion of mast cells gradually increased (R = 0.23, Figure 6B). In particular, SOD2 was highly associated with infiltration of M1 macrophages and CD8+ T cells. The seven genes utilized to build the risk score were strongly connected with numerous immune cell infiltrations (Figure 6C). The monocyte and mast cell infiltration was greater in the low-risk group (Figure 6D). This shows that mast cell suppression may play a significant role in the poor prognosis for LGG. We discovered that practically all immune checkpoints, including CTLA-4, HAVCR2 (TIM3), PDCD1 (PD-1), TIGIT, and CD70, displayed greater activity in the high-risk group by comparing immune checkpoint activation between various risk groups (Figure 6E). Additionally, we were able to determine the stromal score and immunological score of the high-risk and low-risk groups using estimatescore of the expression profile (Figure 6F).

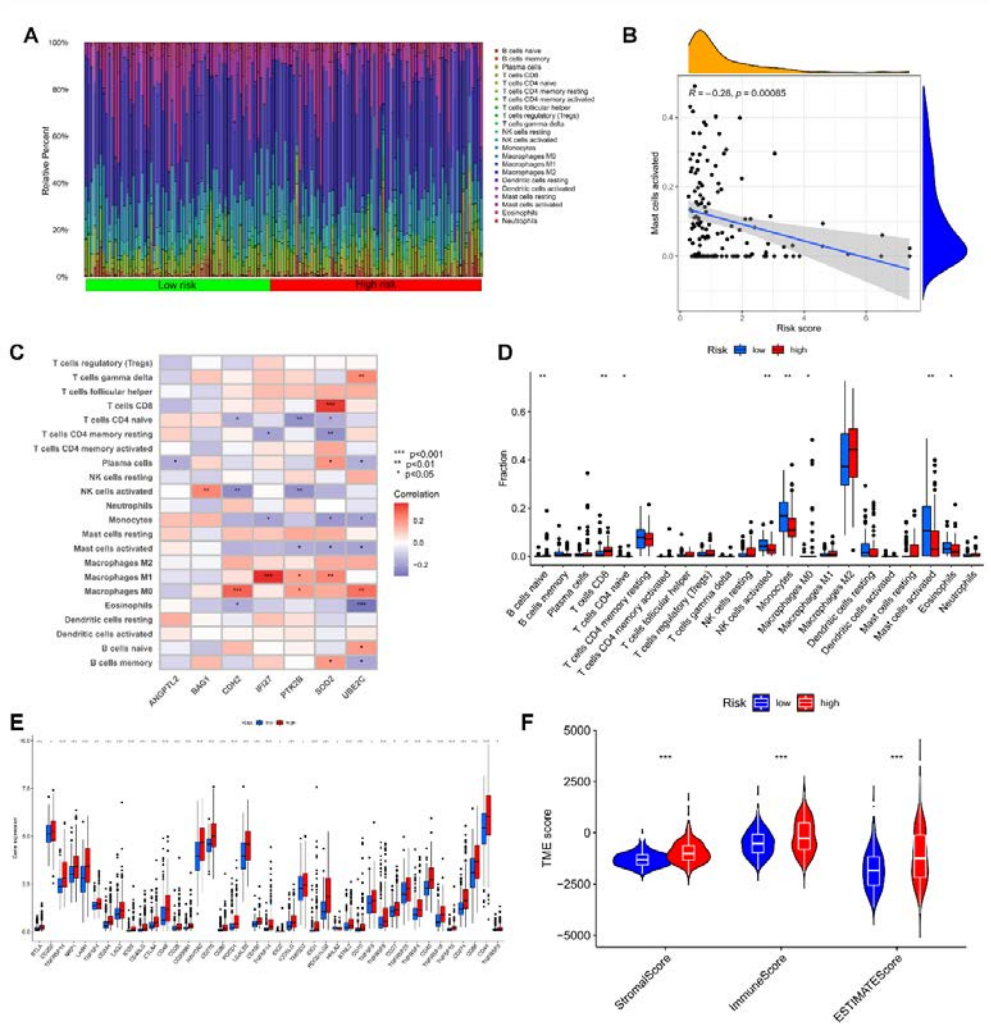

Figure 6. The immune microenvironment of LGG tissues with different risk scores. (A) Relative proportions of infiltrating immune cells with different risk scores. (B) Correlation analysis between risk scores and the proportion of activated Mast cells in LGG tissues. (C) Correlation between immune cells and seven hub ANRGs. (D) Immune cell composition between the high-risk and low-risk groups. (E)Checkpoint expression in the risk groups. (F) Estimatescore of the expression profile in the high-risk group and low-risk group.

3.6. Establishment of a Prognostic Nomogram for LGG Patients

 doi:10.20944/preprints202209.0342.v1

The risk score was identified as an independent predictive factor for LGG in the TCGA population by univariate and multivariate Cox analyses (Figure 7A, B). Then, we included information about risk groups, IDH mutation status, 1p/19q deletion status, tumor grade, age, grade, and tumor grade in the nomogram (Figure 7C). To evaluate the consistency between the prognostic model's predicted overall survival (OS) and the actual overall survival, calibration plots were created. The findings revealed that the nomogram's predictions were accurate (Figure 7D). The efficacy of the created model in accurately predicting OS in LGG patients was evaluated using time-dependent ROC curves. Concerning predicting OS in the TCGA cohort, the risk score did well (AUCs for 1-year, 3-year, and Time-dependent ROC curves were used to assess the accuracy of the developed model for predicting OS in LGG patients. The risk score did well in the TCGA cohort at predicting OS in these people (AUCs for 1-year, 3-year, and 5-year OS: 0.872, 0.844, and 0.813; Figure 7E). Comparable outcomes were seen in the CGGA cohort (Figure 7H). In both the TCGA and CGGA cohorts, the three-year area under the curve (AUC) of the risk score was larger than the AUC of other clinicopathological characteristics (Figure 7F, I). The three-year DCA curves showed that the risk score was a good predictor of survival in LGG patients (Figure 7G, J).

Based on these observations, we compared in detail whether risk scores differed across subgroups of clinical characteristics. We found that individuals with older age, G3 stage, no mutation in IDH, no common defect in 1p/19q, and astrocytoma tissue type showed higher risk scores (Figure 8A-F, P all < 0.05).

Preprints (www.preprints.org) | NOT PEER-REVIEWED | Posted: 22 September 2022 doi:10.20944/preprints202209.0342.v1

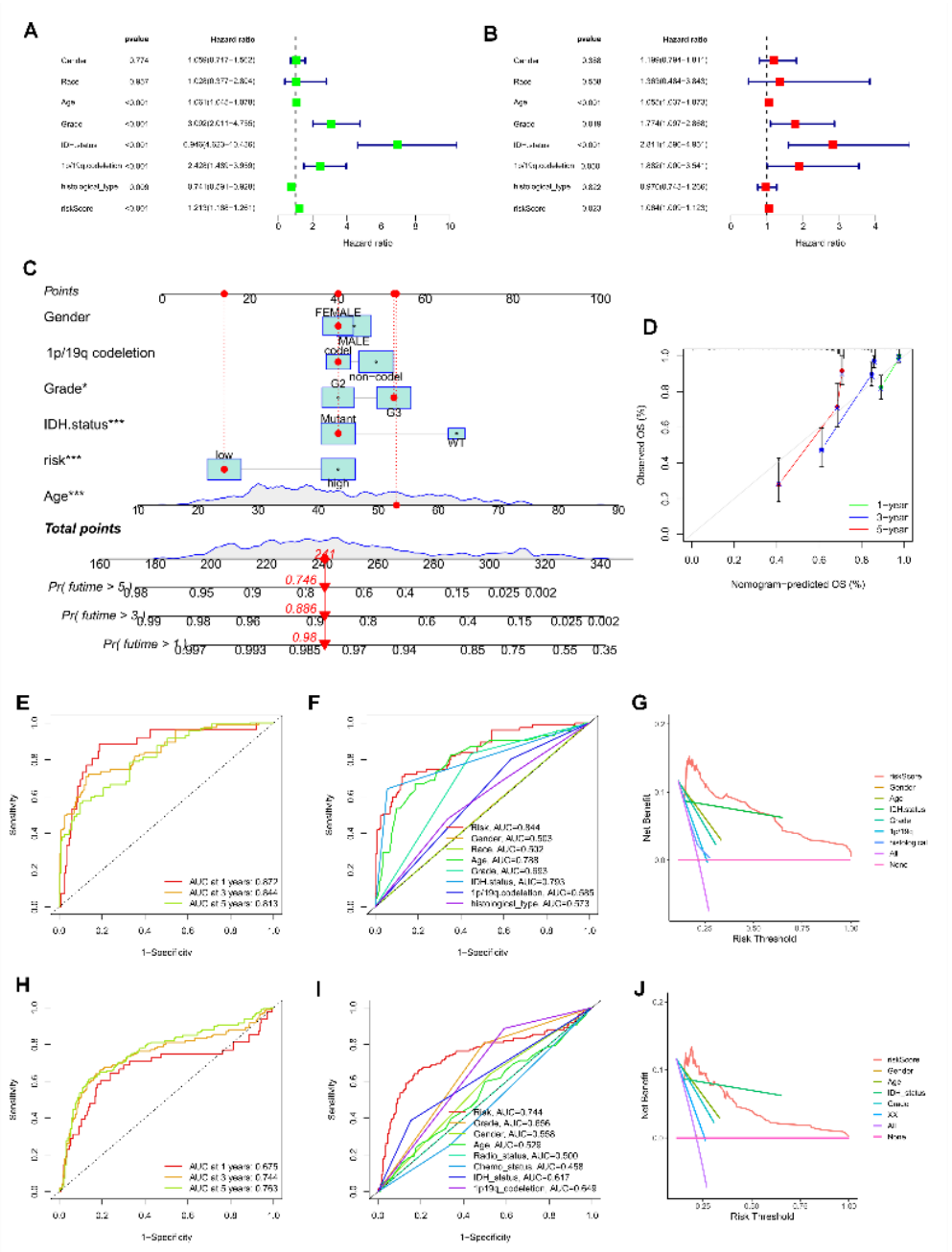

Figure 7. Prognostic value of risk scores in patients with LGG. TCGA cohort (A) Univariate and (B) multi-variate COX analysis to assess risk scores and clinical features (including age, grade, gender, IDH status, and 1p/19q. codeletion). (C) Nomogram of risk groupings and clinical characteristics predicting 1-, 3-, and 5-year survival. (D) Calibration curves tested for agreement between actual and predicted outcomes at 1, 3and5 years. AUC values for the (E)TCGA and (H)CGGA cohort risk scores at 1, 3and5 years. AUC values for (F)TCGA and (I)CGGA cohort risk scores and clinical characteristics at 3 years. DCA curves of risk scores and clinical characteristics for the (G) TCGA and (J) CGGA cohorts at 3 years.

Preprints (www.preprints.org) | NOT PEER-REVIEWED | Posted: 22 September 2022 doi:10.20944/preprints202209.0342.v1

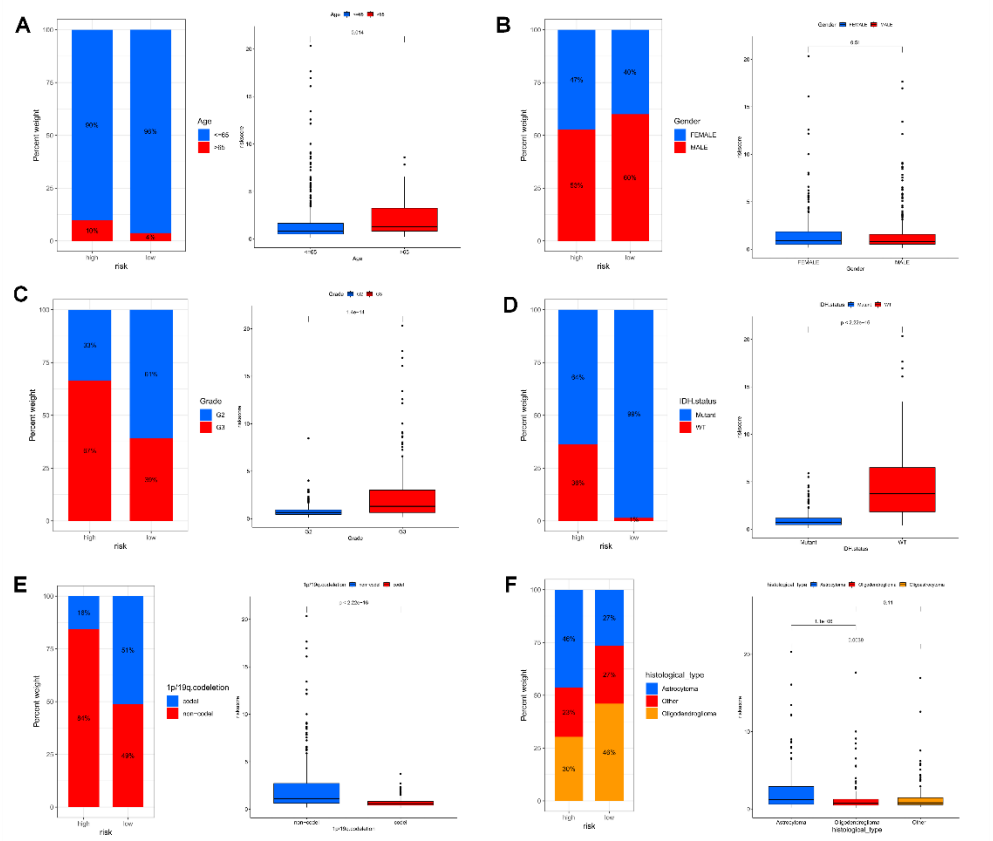

Figure 8. Differences in risk scores among different clinical characteristics subgroups in the TCGA cohort. (A) age, (B) gender, (C) grade, (D) IDH mutation status, (E) 1p/19q. codeletion and (F) histological type. *p < 0.05, **p < 0.01, ***p < 0.001.

3.7. Mutation Landscape in Different Risk Groups

TMB was higher in the high-risk group, according to our analysis of the relationship between risk score and tumor mutation load (TMB) (Figure 9B) and the variation in TMB among various risk groups (Figure 9A). IDH1, TP53, and ATRX were the most frequently mutated genes in high-risk and low-risk groups, respectively (Figure 9C, D). However, there were fewer IDH mutations and more mutations in other genes in the high-risk group. As a result, we generated two waterfall plots to explore the detailed gene mutation characteristics between high- and low-risk populations.

Preprints (www.preprints.org) | NOT PEER-REVIEWED | Posted: 22 September 2022 doi:10.20944/preprints202209.0342.v1

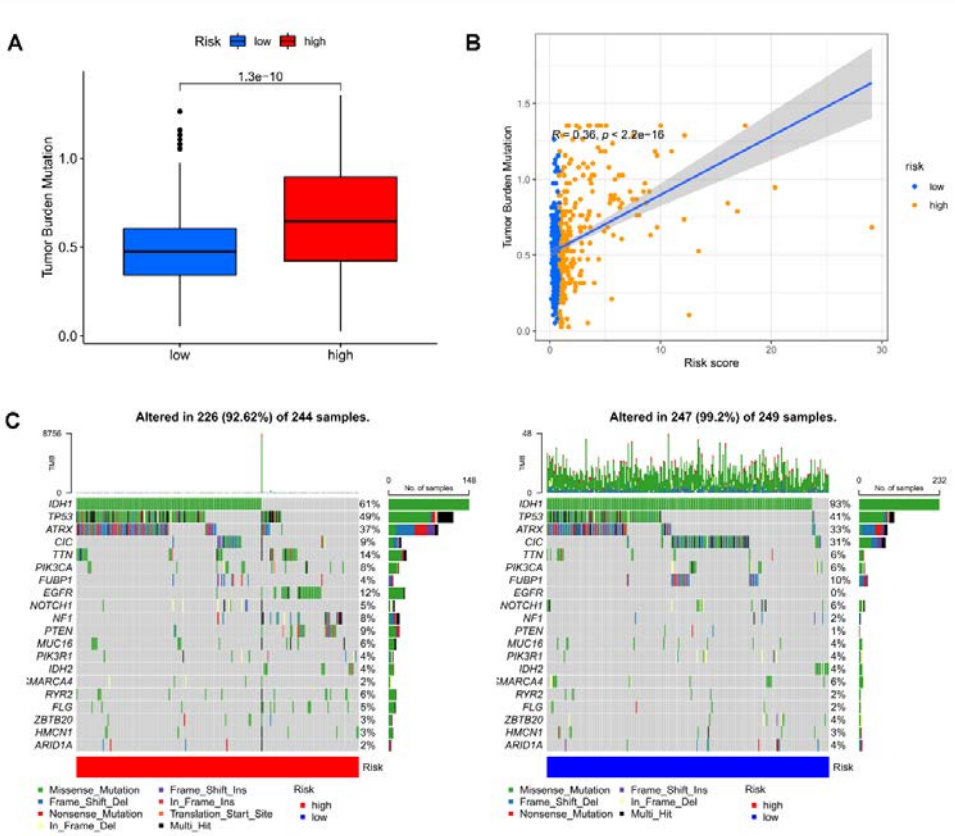

Figure 9. Mutation analysis based on risk score model. (A) Differences in tumor mutational load (TMB) in high-flying risk score groups. (B) Correlation of risk score and TMB. (C, D) Waterfall plots summarizing the mutations in high- and low-risk patients.

3.8. Immunotherapy and ICB Response

Since the immune microenvironment mediates the ICB response, we further analyzed the correlation between risk score and ICB response signature and found that risk score was significantly negatively correlated with Alcoholism only, while it was significantly positively correlated with other ICB response signatures (Figure 10A). Subsequently, to further refine the immune signature of the tumor microenvironment, we also performed a correlation analysis between tumor immune cycle steps and risk score. Once more, risk scores were significantly and favorably correlated with the majority of the critical stages of the tumor immune cycle, such as the release of cancer cell antigen (step 1), presentation of cancer antigen (step 2), priming and activation (step 3), immune cell transport to the tumor (step 4) (CD8 T cell recruitment, Th1 cell recruitment, Th22 cell recruitment, NK cell recruitment, and Th17 cell recruitment), infiltration of immune cells into tumors (step 5), and recognition of cancer (Figure10 B).

Finally, we investigated the potential sensitivity of clinical agents in the high-risk and low-risk groups using the "pRRophetic" R package and screened some chemotherapeutic agents that could be used to treat gliomas, such as lapatinib and afatinib (Figure 10C and D). Almost all of these agents showed higher IC50 in patients with high scores (Supplementary Figure S2), indicating that patients with high-risk scores may be more sensitive.

Preprints (www.preprints.org) | NOT PEER-REVIEWED | Posted: 22 September 2022 doi:10.20944/preprints202209.0342.v1

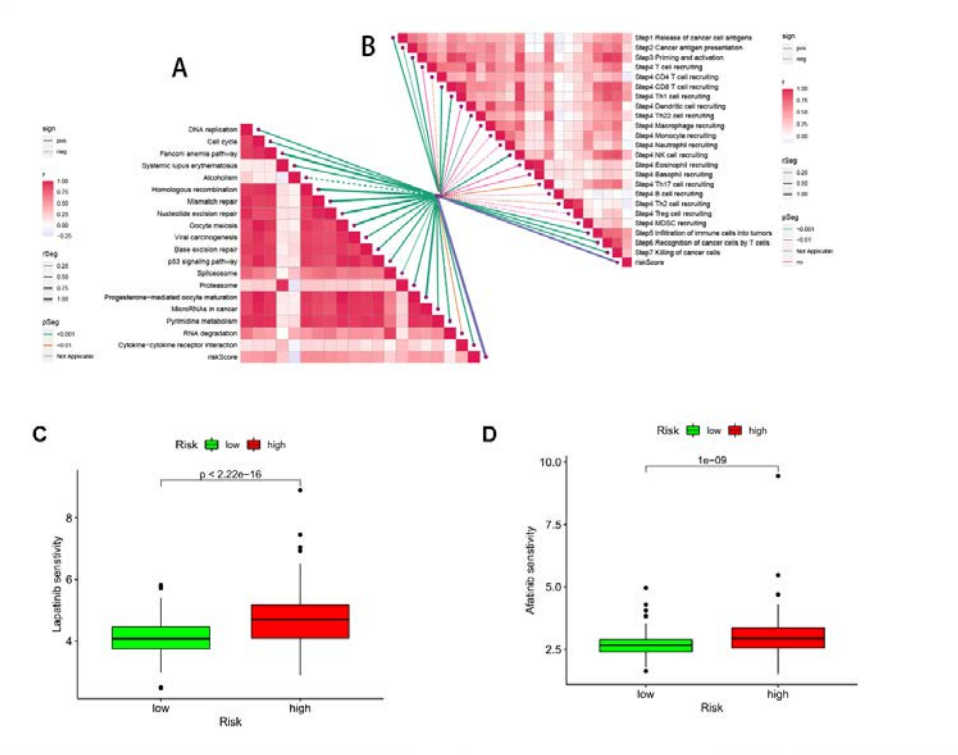

Figure 10. (A) Correlation between risk score and ICB response signature, and (B) correlation between risk score and each step of the tumor immune cycle. IC50 values were calculated for patients in the high- and low-risk groups based on lapatinib (C) and afatinib (D) to assess the sensitivity of chemotherapeutic agents.

3.9. Correlation Analysis of Anoikis-Related Genes and Tumor Immune Microenvironment

To examine the expression of seven ANRGs in TME, we used the single-cell dataset GSE70630 of oligodendroglioma from the TISCH database. There are 10 cell populations and 4 intermediate cell types in the GSE70630 dataset, and the image depicts their distribution and number (Figure 11A). Both PTK2B and SOD2 were mostly expressed in monocyte macrophages, as was discovered. ANGPTL2, BAG1, and CDH2 on the other hand were primarily expressed in cancerous cells and oligodendrocytes (Figure11B, C).

Preprints (www.preprints.org) | NOT PEER-REVIEWED | Posted: 22 September 2022 doi:10.20944/preprints202209.0342.v1

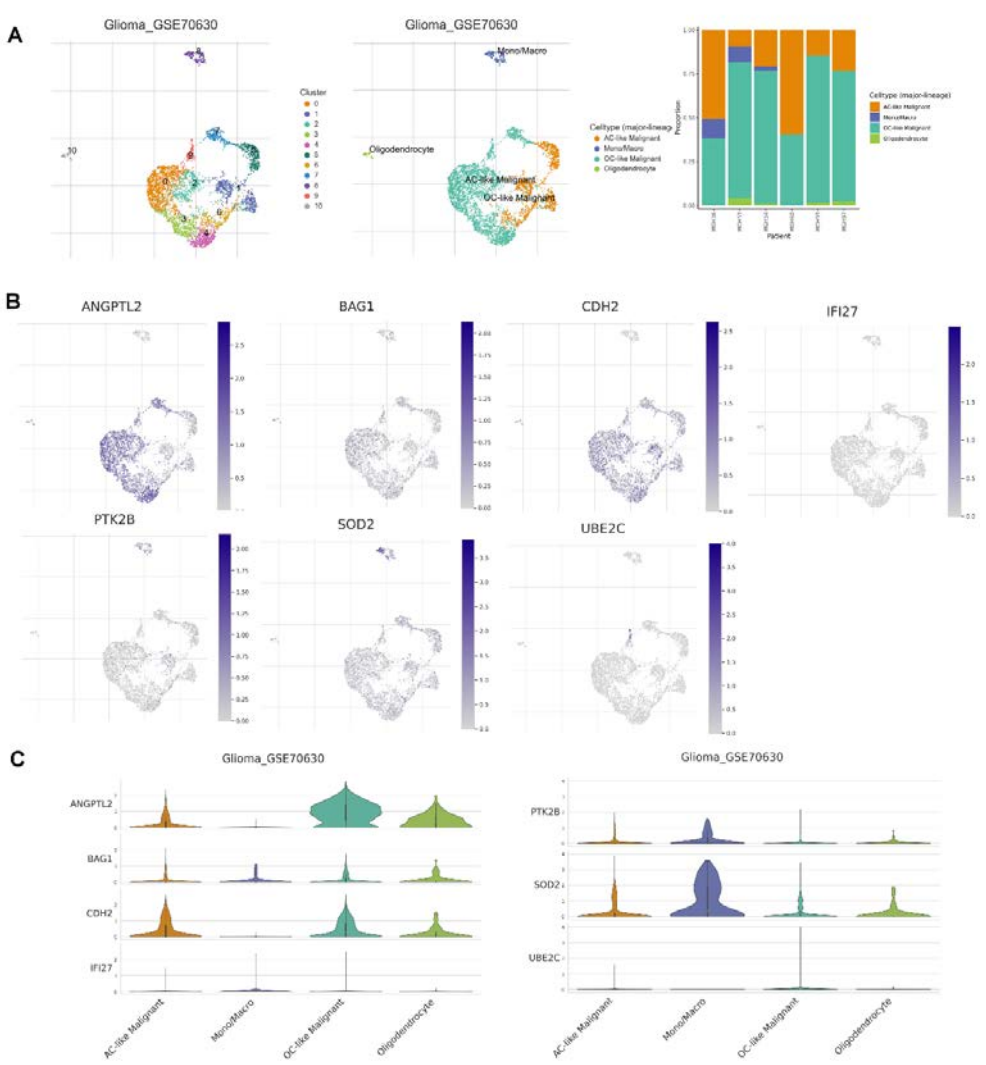

Figure 11. ARHGAP protein family genes in single-cell RNA sequencing (A) Annotation of all cell types in GSE70630 and the percentage of each cell type. (B, C) Percentages and expressions of ANGPTL2, BAG1, CDH2, IFI27, PTK2B, SOD2, and UBE2C.

4. Discussion

The prognosis for glioma patients does not significantly improve despite breakthroughs in surgery, radiation therapy, chemotherapy, and other treatments. Glioma is the most prevalent kind of malignant brain tumor in adults[26,27]. Glioma cells can penetrate along blood vessels and invade surrounding normal brain tissue, making it difficult to remove the tumor as a whole[28]. Once a low-grade glioma differentiates into a high-grade malignant glioblastoma, the invasive ability is enhanced and it can infiltrate and metastasize through the normal tissue space[29]. However, due to the heterogeneity of gliomas and the lack of sustained response, targeted therapies for LGG patients are less effective, and therefore, there is an urgent need for more tumor metastasis-related markers for early glioma treatment to improve diagnostic accuracy.

In the absence of extracellular matrix (ECM) attachment or when cells adhere to inappropriate sites, cells undergo a specific type of apoptosis called anoikis[30]. Failure to properly execute the anoikis program may lead to rapid cell proliferation at ectopic sites. This dysregulation of apoptotic execution is becoming a hallmark of cancer cells and contributes to their metastasis to distant organs[31].

The crucial process by which epithelial cells transform into mesenchymal cells and lose their cell polarity and adhesion is known as oncogenic epithelial-mesenchymal transition (EMT). EMT has recently been discovered in glioma stem cells to directly impact

 doi:10.20944/preprints202209.0342.v1

migration, invading ability, and radiation resistance in gliomas[32]. One of the hallmarks of EMT is the resistance of tumor cells to anoikis. The development of new cancer treatment modalities to address tumor resistance to anoikis has become a hot topic of research in recent years[33,34]. Gliomas have anoikis-resistant properties that enhance their invasion of the adjacent brain parenchyma and eventually recur despite the use of standard therapies. Further exploration regarding the mechanisms of anoikis in gliomas remains to be done. A recent study found that activation of anoikis in glioma cells was associated with inhibition of p21-activated kinase 4 (PAK4)[35]. In addition, Jiang et al. found that MNX1 is bound to the upstream regulatory region of TrkB as a transcription factor to activate its expression, enhancing the ability of glioma cells to evade anoikis[28].

In this work, we found seven genes—ANGPTL2, BAG1, CDH2, IFI27, PTK2B, SOD2, and UBE2C—that together make up robust risk score characteristics. Numerous correlations between these anoikis-related genes and tumorgenesis and pathogenesis have been extensively reported in previous research. Increased ANGPTL2 expression in colorectal cancer (CRC) cells improves -catenin pathway signaling and boosts tumor cell proliferation. ANGPTL2 regulates epithelial regeneration and intestinal immune response[36]. In ovarian cancer, ANGPTL2 can even reduce peritoneal metastasis of tumor cells by inhibiting anoikis resistance[37]. While BAG1 is a multifunctional protein associated with a variety of cellular processes, such as apoptosis, proliferation, growth, and motility[38]. As an autophagy-related gene, BAG1 is also considered to be an important prognostic factor in low-grade gliomas[39]. In colon cancer, knockdown of the neurotrophic factor BDNF suppresses the expression of the mesenchymal marker CDH2 leading to anoikis and immune resistance in tumor cells[40]. Atypical EGFR signaling in glioblastoma activates the transcription factor IRF3, leading to the expression of IFI27, which often plays an important oncogenic role[41]. Acute lymphoblastic leukemia (ALL) contains multiple activated kinase and cytokine receptor signatures, such as genomic alterations in PTK2B[42].

Normal cells require adherence to the extracellular matrix to survive. Cell shedding leads to a dramatic increase in reactive oxygen species (ROS), which promotes anoikis[43,44]. And mammary epithelial cells can reduce anoikis by increasing mitochondrial antioxidant enzyme SOD2 to reduce ROS produced by mitochondrial glucose oxidation[45]. Similarly, in ovarian cancer cells, SOD2 protein expression is associated with increased oxidative stress, and ovarian cancer cells rapidly increase their mitochondrial antioxidant capacity through this mechanism as a means to adapt to the loss of anchor points and escape anoikis[46]. Ma et al. found that the ubiquitin-binding enzyme E2C (UBE2C) is a key regulator of cell cycle progression and an important factor in the malignant progression of astrocytic tumors[47]. Meanwhile silencing of UBE2C in glioma leads to significant inhibition of the PI3K-Akt-mTOR pathway, while avoiding autophagy[48].

To evaluate the status of anoikis, we utilized unsupervised cluster analysis to divide LGG patients into three subgroups (clusters A, B, and C) based on 27 ANRGs. The majority of the ANRGs were discovered to be highly expressed in cluster A, which is likely what caused the individuals in group A to have a worse prognosis. The results imply that anoikis can affect how LGGs form. The two clusters of AB differed in tumor infiltration and metastasis-related pathways, according to GSVA. In the current study7, both the training and validation cohorts of LGG patients showed that the anoikis-related gene signature correctly predicted OS. This gene signature was an independent predictor of LGG prognosis in both the TCGA and CGGA cohorts when considering relevant clinical characteristics, such as tumor grade, age, and sex. Clinical variables with high-risk scores tended to be statistically significant risk factors for prognosis, suggesting that the ANRG gene signature could be a predictor of prognosis and could be a proxy for prognosis. Patients with concurrent risk scores tended to have higher tumor grade, IDH-wild type, and no 1p/19q co-deletion, which is consistent with previous studies[49,50] and more suggestive of a high-risk adverse prognostic profile.

To investigate the prognostic mechanism of this feature and to provide clues for predicting ICI, we compared the high-risk and low-risk groups in terms of the proportion of 22 immune cells, TME, gene mutations, and TMB. Consistent with previous studies, CD8+

 doi:10.20944/preprints202209.0342.v1

T-cell infiltration was greater in the high-risk group. Furthermore, SOD2, among the seven risk genes, had the highest correlation coefficient with CD8+ T cells[51]. Thus, SOD2 activation of the CD8+T cell axis may be an interesting pathway. We also found that the high-risk group exhibited higher TMB than the low-risk group, but the low-risk group expressed more high-frequency IDH and CIC mutations[52]. The high-risk group showed higher TMB, which would lead to more neoantigens and enhanced T-cell recognition, and therefore could be a good predictor of the effect of ICI therapy.

In 2013, Chen and Mellman introduced the concept of tumor immune cycling. Tumor immunity arises as a continuously self-derived cyclic process, through which immune stimulatory molecules are accumulated to amplify T cell responses[53]. Thus, the cancer-immune cycle represents the immune response of the human immune system to cancer. Immune checkpoint inhibitors, particularly treatments such as anti-PD-1/PD-L1 and CTLA-4, are effective against a wide range of tumors but have performed poorly in clinical trials in glioma[54]. The efficacy of immunotherapy in glioma is associated with its unique molecular alterations, immune expression profile, and immune infiltration, and correlates with a high level of the immune microenvironment and immune checkpoint expression in the tumor. In addition patients in the high-risk group tended to have higher immune checkpoint gene expression, while we found a significant correlation between higher risk scores and both the tumor immune cycle and ICB response so that patients in the high-risk group were in inflammatory TME[55]. while patients with high-risk LGG can have better immunotherapy outcomes.

5. Conclusion

In conclusion, our 7 anoikis-related genes signature can well predict the survival of LGG patients, and it will assist clinicians in creating various treatment plans. The DCA curve also indicates that LGG patients can benefit from the nomogram created using the 7 genes signature. In practical practice, columnar maps based on this concept can aid doctors in creating personalized treatments. Our study still has some inherent problems, though. Future experimental confirmation is required because all of these conclusions came from bioinformatics research.

Supplementary Materials: The following supporting information can be downloaded at: www.mdpi.com/xxx/s1, Figure S1: GSVA analysis of clusters B (or A) and C.; Figure S2: A drug sensitivity analysis.

Author Contributions: Conceptualization, C.C. , W.H. , X.Z. , and G.L.; methodology, S.Z. , H.C.; software, S.Z.; formal analy-sis, G.P.; data curation, W.J. , Q.H., and H.C.; writing—original draft preparation, H.C., S.Z and G.L.; writing—review and editing, W.J., H.C.; visualization, S.Z.; funding acquisition, C.C. All authors have read and agreed to the published version of the manuscript.

Funding: This work was supported by Wuxi Taihu Lake Talent Plan, Supports for Leading Talents in Medical and Health Profession（2020THRC-DJ-SNW）, General project of Wuxi commission of Health(2020ZHYB16, MS201933, T202120).

Data Availability Statement: The datasets analyzed in this study can be found in the TCGA-LGG project (http://www.cancer.gov/tcga), CGGA database (http://www.cgga.org.cn/), and GTEx project (https://gtexportal.org/home/).

Conflicts of Interest: The authors declare no conflict of in-terest.

References

1. Yang, Y.; Liu, X.; Cheng, L.; Li, L.; Wei, Z.; Wang, Z.; Han, G.; Wan, X.; Wang, Z.; Zhang, J.; et al. Tumor Suppressor microRNA-138 Suppresses Low-Grade Glioma Development and Metastasis via Regulating IGF2BP2. *Onco Targets Ther* **2020**, *13*, 2247-2260, doi:10.2147/OTT.S232795.
2. Baumert, B.G.; Hegi, M.E.; van den Bent, M.J.; von Deimling, A.; Gorlia, T.; Hoang-Xuan, K.; Brandes, A.A.; Kantor, G.; Taphoorn, M.J.B.; Hassel, M.B.; et al. Temozolomide chemotherapy versus radiotherapy in high-risk low-grade glioma (EORTC 22033-26033): a randomised, open-label, phase 3 intergroup study. *Lancet Oncol* **2016**, *17*, 1521-1532, doi:10.1016/S1470-2045(16)30313-8.
3. Lewis, B.P.; Burge, C.B.; Bartel, D.P. Conserved seed pairing, often flanked by adenosines, indicates that thousands of human genes are microRNA targets. *Cell* **2005**, *120*, 15-20, doi:10.1016/j.cell.2004.12.035.
4. Liu, R.; Solheim, K.; Polley, M.Y.; Lamborn, K.R.; Page, M.; Fedoroff, A.; Rabbitt, J.; Butowski, N.; Prados, M.; Chang, S.M. Quality of life in low-grade glioma patients receiving temozolomide. *Neuro Oncol* **2009**, *11*, 59-68, doi:10.1215/15228517-2008-063.
5. Hersh, D.S.; Harder, B.G.; Roos, A.; Peng, S.; Heath, J.E.; Legesse, T.; Kim, A.J.; Woodworth, G.F.; Tran, N.L.; Winkles, J.A. The TNF receptor family member Fn14 is highly expressed in recurrent glioblastoma and in GBM patient-derived xenografts with acquired temozolomide resistance. *Neuro Oncol* **2018**, *20*, 1321-1330, doi:10.1093/neuonc/noy063.
6. Delgado-Martin, B.; Medina, M.A. Advances in the Knowledge of the Molecular Biology of Glioblastoma and Its Impact in Patient Diagnosis, Stratification, and Treatment. *Adv Sci (Weinh)* **2020**, *7*, 1902971, doi:10.1002/advs.201902971.
7. Chiarugi, P.; Giannoni, E. Anoikis: a necessary death program for anchorage-dependent cells. *Biochem Pharmacol* **2008**, *76*, 1352-1364, doi:10.1016/j.bcp.2008.07.023.
8. Boudreau, N.J.; Jones, P.L. Extracellular matrix and integrin signalling: the shape of things to come. *Biochem J* **1999**, *339 (Pt 3)*, 481-488.
9. Frisch, S.M.; Ruoslahti, E. Integrins and anoikis. *Curr Opin Cell Biol* **1997**, *9*, 701-706, doi:10.1016/s0955-0674(97)80124-x.
10. Kim, Y.N.; Koo, K.H.; Sung, J.Y.; Yun, U.J.; Kim, H. Anoikis resistance: an essential prerequisite for tumor metastasis. *Int J Cell Biol* **2012**, *2012*, 306879, doi:10.1155/2012/306879.
11. Yu, Y.; Song, Y.; Cheng, L.; Chen, L.; Liu, B.; Lu, D.; Li, X.; Li, Y.; Lv, F.; Xing, Y. CircCEMIP promotes anoikis-resistance by enhancing protective autophagy in prostate cancer cells. *J Exp Clin Cancer Res* **2022**, *41*, 188, doi:10.1186/s13046-022-02381-7.
12. Leek, J.T.; Johnson, W.E.; Parker, H.S.; Jaffe, A.E.; Storey, J.D. The sva package for removing batch effects and other unwanted variation in high-throughput experiments. *Bioinformatics* **2012**, *28*, 882-883, doi:10.1093/bioinformatics/bts034.
13. Rebhan, M.; Chalifa-Caspi, V.; Prilusky, J.; Lancet, D. GeneCards: integrating information about genes, proteins and diseases. *Trends Genet* **1997**, *13*, 163, doi:10.1016/s0168-9525(97)01103-7.
14. Rouillard, A.D.; Gundersen, G.W.; Fernandez, N.F.; Wang, Z.; Monteiro, C.D.; McDermott, M.G.; Ma'ayan, A. The harmonizome: a collection of processed datasets gathered to serve and mine knowledge about genes and proteins. *Database (Oxford)* **2016**, *2016*, doi:10.1093/database/baw100.
15. Hanzelmann, S.; Castelo, R.; Guinney, J. GSVA: gene set variation analysis for microarray and RNA-seq data. *BMC Bioinformatics* **2013**, *14*, 7, doi:10.1186/1471-2105-14-7.
16. Sanz, H.; Valim, C.; Vegas, E.; Oller, J.M.; Reverter, F. SVM-RFE: selection and visualization of the most relevant features through non-linear kernels. *BMC Bioinformatics* **2018**, *19*, 432, doi:10.1186/s12859-018-2451-4.
17. Newman, A.M.; Liu, C.L.; Green, M.R.; Gentles, A.J.; Feng, W.; Xu, Y.; Hoang, C.D.; Diehn, M.; Alizadeh, A.A. Robust enumeration of cell subsets from tissue expression profiles. *Nat Methods* **2015**, *12*, 453-457, doi:10.1038/nmeth.3337.
18. Xu, L.; Deng, C.; Pang, B.; Zhang, X.; Liu, W.; Liao, G.; Yuan, H.; Cheng, P.; Li, F.; Long, Z.; et al. TIP: A Web Server for Resolving Tumor Immunophenotype Profiling. *Cancer Res* **2018**, *78*, 6575-6580, doi:10.1158/0008-5472.CAN-18-0689.
19. Mariathasan, S.; Turley, S.J.; Nickles, D.; Castiglioni, A.; Yuen, K.; Wang, Y.; Kadel, E.E., III; Koeppen, H.; Astarita, J.L.; Cubas, R.; et al. TGFbeta attenuates tumour response to PD-L1 blockade by contributing to exclusion of T cells. *Nature* **2018**, *554*, 544-548, doi:10.1038/nature25501.
20. Vickers, A.J.; Cronin, A.M.; Elkin, E.B.; Gonen, M. Extensions to decision curve analysis, a novel method for evaluating diagnostic tests, prediction models and molecular markers. *BMC Med Inform Decis Mak* **2008**, *8*, 53, doi:10.1186/1472-6947-8-53.
21. Sun, D.; Wang, J.; Han, Y.; Dong, X.; Ge, J.; Zheng, R.; Shi, X.; Wang, B.; Li, Z.; Ren, P.; et al. TISCH: a comprehensive web resource enabling interactive single-cell transcriptome visualization of tumor microenvironment. *Nucleic Acids Res* **2021**, *49*, D1420-D1430, doi:10.1093/nar/gkaa1020.
22. Reiter, J.G.; Baretti, M.; Gerold, J.M.; Makohon-Moore, A.P.; Daud, A.; Iacobuzio-Donahue, C.A.; Azad, N.S.; Kinzler, K.W.; Nowak, M.A.; Vogelstein, B. An analysis of genetic heterogeneity in untreated cancers. *Nat Rev Cancer* **2019**, *19*, 639-650, doi:10.1038/s41568-019-0185-x.
23. Lewis-Tuffin, L.J.; Rodriguez, F.; Giannini, C.; Scheithauer, B.; Necela, B.M.; Sarkaria, J.N.; Anastasiadis, P.Z. Misregulated E-cadherin expression associated with an aggressive brain tumor phenotype. *PLoS One* **2010**, *5*, e13665, doi:10.1371/journal.pone.0013665.
24. Tseng, T.; Uen, W.; Tseng, J.; Lee, S. Enhanced chemosensitization of anoikis-resistant melanoma cells through syndecan-2 upregulation upon anchorage independency. *Oncotarget* **2017**, *8*, 61528-61537, doi:10.18632/oncotarget.18616.
25. Carneiro, B.R.; Pernambuco Filho, P.C.; Mesquita, A.P.; da Silva, D.S.; Pinhal, M.A.; Nader, H.B.; Lopes, C.C. Acquisition of anoikis resistance up-regulates syndecan-4 expression in endothelial cells. *PLoS One* **2014**, *9*, e116001, doi:10.1371/journal.pone.0116001.

26. Shen, Y.; Chi, H.; Xu, K.; Li, Y.; Yin, X.; Chen, S.; Yang, Q.; He, M.; Zhu, G.; Li, X. A Novel Classification Model for Lower-Grade Glioma Patients Based on Pyroptosis-Related Genes. *Brain Sci* **2022**, *12*, doi:10.3390/brainsci12060700.
27. Lai, G.; Li, K.; Deng, J.; Liu, H.; Xie, B.; Zhong, X. Identification and Validation of a Gene Signature for Lower-Grade Gliomas Based on Pyroptosis-Related Genes to Predict Survival and Response to Immune Checkpoint Inhibitors. *J Healthc Eng* **2022**, *2022*, 8704127, doi:10.1155/2022/8704127.
28. Jiang, L.; Chen, S.; Zhao, D.; Yan, J.; Chen, J.; Yang, C.; Zheng, G. MNX1 reduces sensitivity to anoikis by activating TrkB in human glioma cells. *Mol Med Rep* **2018**, *18*, 3271-3279, doi:10.3892/mmr.2018.9329.
29. Douma, S.; Van Laar, T.; Zevenhoven, J.; Meuwissen, R.; Van Garderen, E.; Peeper, D.S. Suppression of anoikis and induction of metastasis by the neurotrophic receptor TrkB. *Nature* **2004**, *430*, 1034-1039, doi:10.1038/nature02765.
30. Bakir, B.; Chiarella, A.M.; Pitarresi, J.R.; Rustgi, A.K. EMT, MET, Plasticity, and Tumor Metastasis. *Trends Cell Biol* **2020**, *30*, 764-776, doi:10.1016/j.tcb.2020.07.003.
31. Taddei, M.L.; Giannoni, E.; Fiaschi, T.; Chiarugi, P. Anoikis: an emerging hallmark in health and diseases. *J Pathol* **2012**, *226*, 380-393, doi:10.1002/path.3000.
32. Lah, T.T.; Novak, M.; Breznik, B. Brain malignancies: Glioblastoma and brain metastases. *Semin Cancer Biol* **2020**, *60*, 262-273, doi:10.1016/j.semcancer.2019.10.010.
33. Tiwari, N.; Gheldof, A.; Tatari, M.; Christofori, G. EMT as the ultimate survival mechanism of cancer cells. *Semin Cancer Biol* **2012**, *22*, 194-207, doi:10.1016/j.semcancer.2012.02.013.
34. Mjones, S. [Look systematically for malaria in exposed children]. *Lakartidningen* **1990**, *87*, 1965-1966.
35. Kesanakurti, D.; Chetty, C.; Rajasekhar Maddirela, D.; Gujrati, M.; Rao, J.S. Functional cooperativity by direct interaction between PAK4 and MMP-2 in the regulation of anoikis resistance, migration and invasion in glioma. *Cell Death Dis* **2012**, *3*, e445, doi:10.1038/cddis.2012.182.
36. Horiguchi, H.; Kadomatsu, T.; Yumoto, S.; Masuda, T.; Miyata, K.; Yamamura, S.; Sato, M.; Morinaga, J.; Ohtsuki, S.; Baba, H.; et al. Tumor cell-derived ANGPTL2 promotes beta-catenin-driven intestinal tumorigenesis. *Oncogene* **2022**, *41*, 4028-4041, doi:10.1038/s41388-022-02405-8.
37. Takeshita, Y.; Motohara, T.; Kadomatsu, T.; Doi, T.; Obayashi, K.; Oike, Y.; Katabuchi, H.; Endo, M. Angiopoietin-like protein 2 decreases peritoneal metastasis of ovarian cancer cells by suppressing anoikis resistance. *Biochem Biophys Res Commun* **2021**, *561*, 26-32, doi:10.1016/j.bbrc.2021.05.008.
38. Ostrom, Q.T.; Gittleman, H.; Farah, P.; Ondracek, A.; Chen, Y.; Wolinsky, Y.; Stroup, N.E.; Kruchko, C.; Barnholtz-Sloan, J.S. CBTRUS statistical report: Primary brain and central nervous system tumors diagnosed in the United States in 2006-2010. *Neuro Oncol* **2013**, *15 Suppl 2*, ii1-56, doi:10.1093/neuonc/not151.
39. Lin, T.; Cheng, H.; Liu, D.; Wen, L.; Kang, J.; Xu, L.; Shan, C.; Chen, Z.; Li, H.; Lai, M.; et al. A Novel Six Autophagy-Related Genes Signature Associated With Outcomes and Immune Microenvironment in Lower-Grade Glioma. *Front Genet* **2021**, *12*, 698284, doi:10.3389/fgene.2021.698284.
40. Ha, C.T.; Cheng, C.Y.; Zheng, M.Y.; Hsu, T.H.; Miao, C.C.; Lee, C.J.; Wang, H.D.; Pan, S.T.; Chou, Y.T. ID4 predicts poor prognosis and promotes BDNF-mediated oncogenesis of colorectal cancer. *Carcinogenesis* **2021**, *42*, 951-960, doi:10.1093/carcin/bgab037.
41. Chakraborty, S.; Li, L.; Puliyappadamba, V.T.; Guo, G.; Hatanpaa, K.J.; Mickey, B.; Souza, R.F.; Vo, P.; Herz, J.; Chen, M.R.; et al. Constitutive and ligand-induced EGFR signalling triggers distinct and mutually exclusive downstream signalling networks. *Nat Commun* **2014**, *5*, 5811, doi:10.1038/ncomms6811.
42. Tasian, S.K.; Loh, M.L.; Hunger, S.P. Philadelphia chromosome-like acute lymphoblastic leukemia. *Blood* **2017**, *130*, 2064-2072, doi:10.1182/blood-2017-06-743252.
43. Sousa, B.; Pereira, J.; Marques, R.; Grilo, L.F.; Pereira, S.P.; Sardao, V.A.; Schmitt, F.; Oliveira, P.J.; Paredes, J. P-cadherin induces anoikis-resistance of matrix-detached breast cancer cells by promoting pentose phosphate pathway and decreasing oxidative stress. *Biochim Biophys Acta Mol Basis Dis* **2020**, *1866*, 165964, doi:10.1016/j.bbadis.2020.165964.
44. Kim, Y.S.; Gupta Vallur, P.; Jones, V.M.; Worley, B.L.; Shimko, S.; Shin, D.H.; Crawford, L.C.; Chen, C.W.; Aird, K.M.; Abraham, T.; et al. Context-dependent activation of SIRT3 is necessary for anchorage-independent survival and metastasis of ovarian cancer cells. *Oncogene* **2020**, *39*, 1619-1633, doi:10.1038/s41388-019-1097-7.
45. Kamarajugadda, S.; Cai, Q.; Chen, H.; Nayak, S.; Zhu, J.; He, M.; Jin, Y.; Zhang, Y.; Ai, L.; Martin, S.S.; et al. Manganese superoxide dismutase promotes anoikis resistance and tumor metastasis. *Cell Death Dis* **2013**, *4*, e504, doi:10.1038/cddis.2013.20.
46. Kim, Y.S.; Tang, P.W.; Welles, J.E.; Pan, W.; Javed, Z.; Elhaw, A.T.; Mythreye, K.; Kimball, S.R.; Hempel, N. HuR-dependent SOD2 protein synthesis is an early adaptation to anchorage-independence. *Redox Biol* **2022**, *53*, 102329, doi:10.1016/j.redox.2022.102329.
47. Ma, R.; Kang, X.; Zhang, G.; Fang, F.; Du, Y.; Lv, H. High expression of UBE2C is associated with the aggressive progression and poor outcome of malignant glioma. *Oncol Lett* **2016**, *11*, 2300-2304, doi:10.3892/ol.2016.4171.
48. Guo, L.; Ding, Z.; Huang, N.; Huang, Z.; Zhang, N.; Xia, Z. Forkhead Box M1 positively regulates UBE2C and protects glioma cells from autophagic death. *Cell Cycle* **2017**, *16*, 1705-1718, doi:10.1080/15384101.2017.1356507.
49. Chiocca, E.A.; Yu, J.S.; Lukas, R.V.; Solomon, I.H.; Ligon, K.L.; Nakashima, H.; Triggs, D.A.; Reardon, D.A.; Wen, P.; Stopa, B.M.; et al. Regulatable interleukin-12 gene therapy in patients with recurrent high-grade glioma: Results of a phase 1 trial. *Sci Transl Med* **2019**, *11*, doi:10.1126/scitranslmed.aaw5680.

50. Bangalore Yogananda, C.G.; Shah, B.R.; Vejdani-Jahromi, M.; Nalawade, S.S.; Murugesan, G.K.; Yu, F.F.; Pinho, M.C.; Wagner, B.C.; Mickey, B.; Patel, T.R.; et al. A novel fully automated MRI-based deep-learning method for classification of IDH mutation status in brain gliomas. *Neuro Oncol* **2020**, *22*, 402-411, doi:10.1093/neuonc/noz199.
51. Luo, C.; Liu, Z.; Ye, W.; Liu, F. Immune Infiltration-Related Signature Predicts Risk Stratification and Immunotherapy Efficacy in Grade II and III Gliomas. *Front Cell Dev Biol* **2021**, *9*, 756005, doi:10.3389/fcell.2021.756005.
52. Chan, T.A.; Yarchoan, M.; Jaffee, E.; Swanton, C.; Quezada, S.A.; Stenzinger, A.; Peters, S. Development of tumor mutation burden as an immunotherapy biomarker: utility for the oncology clinic. *Ann Oncol* **2019**, *30*, 44-56, doi:10.1093/annonc/mdy495.
53. Chen, D.S.; Mellman, I. Oncology meets immunology: the cancer-immunity cycle. *Immunity* **2013**, *39*, 1-10, doi:10.1016/j.immuni.2013.07.012.
54. Yu, J.; Qin, B.; Moyer, A.M.; Nowsheen, S.; Tu, X.; Dong, H.; Boughey, J.C.; Goetz, M.P.; Weinshilboum, R.; Lou, Z.; et al. Regulation of sister chromatid cohesion by nuclear PD-L1. *Cell Res* **2020**, *30*, 590-601, doi:10.1038/s41422-020-0315-8.
55. Denk, D.; Greten, F.R. Inflammation: the incubator of the tumor microenvironment. *Trends Cancer* **2022**, doi:10.1016/j.trecan.2022.07.002.